Hindawi
Shock and Vibration
Volume 2023, Article ID 5409006, 20 pages
https://doi.org/10.1155/2023/5409006

Research Article

Underwater Shaking-Table Investigation of Complex Deep-Water Pile-Cap Foundation for Xihoumen Rail-cum-Road Bridge

Lei Wang,[1,2] **Zhong-da Lv**,[2] **Fei Wang**,[2] **Zhuo Zhao**,[2] **and Xin-long Dong**[1]

[1]*MOE Key Laboratory of Impact and Safety Engineering, Ningbo University, Ningbo 315211, China*
[2]*Engineering Research Center of Industrial Construction in Civil Engineering of Zhejiang Province, Ningbo University of Technology, Ningbo 315211, China*

Correspondence should be addressed to Zhong-da Lv; lzd01@189.cn

Received 26 April 2023; Revised 5 June 2023; Accepted 16 June 2023; Published 23 June 2023

Academic Editor: Xiuquan Liu

To study the mechanical characteristics of complex pile-cap foundations and the distribution law of hydrodynamic pressure acting on piles and cap in deep-water environments, the 60 m deep-water pile-cap foundation of Xihoumen rail-cum-road bridge was considered for this investigation. This paper focused on introducing the design and implementation process of simulating an earthquake using an underwater shaking-table test for a 1 : 60 complex pile-cap foundation model and systematically summarizing the test results. The test results showed that water reduced the acceleration of complex pile-cap foundation; however, the strain, displacement, and hydrodynamic pressure increased in varying degrees with water depths, and the maximum strain of the piles increased by 13.8% for the *X*-direction earthquake excitation and 15.1% for the *Y*-direction earthquake excitation in 1.0 m water-depth environment. The strain of the corner pile was the largest under earthquake excitation, followed by that of the front-row pile, and the strain of the middle pile was the smallest. When the water depth was 1.0 m, the maximum strain difference of each pile in the *X*- and *Y*-directions reached 26.4% and 27.5%, respectively. The hydrodynamic pressure acting on the piles decreased gradually from bottom to top, the edge pile bore more hydrodynamic pressure than the middle pile, and the hydrodynamic pressure difference between the piles reached 20%. Owing to the influence of the round-ended cap, the hydrodynamic pressure suddenly increased at the cap position, and the distribution law of the cap showed a gradually declining trend from front to side; however, the attenuation amplitude was affected by its shape.

1. Introduction

An increasing number of coastal and offshore engineering structures, such as cross-sea bridges, offshore oil platforms, wharfs, and wind-power towers, are being constructed in deep water. The loads from deep-water environments are extremely complex; hence, when exploring the problem of structure-water coupling under earthquake excitation, most current research has focused on theoretical analysis and numerical calculation [1–3]. However, the hydrodynamic pressure and fluid-structure coupling of deep-water structures are arduous to simulate [4, 5]. Based on different understandings of fluid-structure coupling between underwater structures and surrounding water bodies under earthquake excitation and the selection of calculation model parameters, the research results obtained by different researchers are often dissimilar [6–8]. Because of the sudden occurrence of earthquakes and the complexity of field tests in deep-water environments, it is impossible to conduct field research. Therefore, the underwater shaking-table test of scaled models is still considered a reliable and direct research approach that satisfies a similarity ratio relationship [9, 10].

Many studies have used the shaking-table test to obtain the dynamic response of structures, particularly complex or underwater structures. Hazarika et al. [11] conducted a series of large-scale underwater shaking-table tests on waterfront structures, and the experimental results identified that the seismic load against the caisson quay wall could be substantially reduced by a cushioning technique of using the tire chips cushion; in addition, the presence of the protective tire

chip cushion could significantly reduce the earthquake-induced residual displacement of the caisson quay wall. Haddad et al. [12] performed shaking-table model tests to evaluate liquefaction hazards to the behavior of offshore wind turbines, and the results identified the two controversial mechanisms controlling shear-induced caisson settlement; the liquefaction-induced bearing capacity failure as the skirt length of suction caisson increases, whereas the larger net excess pore-water pressures in suction caisson contribute more significantly to reducing seismic demand on wind turbine. At present, underwater shaking-table tests of bridges are less frequent, and the test objects are mostly single pier structures or simple pile-cap foundations [13, 14]. Li et al. [15] conducted a series of shaking-table tests on four circular steel tubes with different diameters, and the main purpose was to determine the inertial coefficient in the Morison equation. The test results showed that the hydrodynamic added mass increased with steel tube diameters and water depths, and a method to calculate the hydrodynamic added mass under the real earthquake was proposed. Huang and Li [16] studied the seismic response of a rectangular bridge pier in different water depths, and the research results indicated that the hydrodynamic pressure effect on the seismic response of bridge piers increased with the increase of the relative water depth; when the water depth was 80% of the pier height, the stress of the pier bottom increased by 21%, and the relative displacement of the pier top increased by 22.4% than that without water. Song et al. [17] performed a pile-cap foundation test on the south pier of the third Nanjing Yangtze River Bridge, the experimental results showed that the maximum acceleration in water increased 20% to 40% than that without water under different seismic waves, and the maximum displacement and strain increased 10% to 20% accordingly. Limited by the test conditions, the test model and water tanks were connected in the above-mentioned test. Although some rules can be obtained, the study still has significant limitations. Liu and Sun [18] studied the natural frequency of concrete pile-cap foundation using the submerged shaking-table system, and the results showed that the natural frequency of pile-cap foundation model decreased by 9.1% in water than that without water. Lai et al. [19] conducted an underwater shaking-table test of a pile-cap foundation according to the approach bridge of the Pingtan Strait Bridge, the results of test shows that compared to that without water, the natural vibration frequency of the model in water was reduced by 2.6%, and the maximum strain at the bottom of the pile increased by 3.0% under Tianjin earthquake and 7.0% under Loma Prieta earthquake, respectively. The layout of the piles was 2×2, and the simulated maximum water depth was 30 m. The test results identified that the water would change the dynamic characteristics and the responses of submerged bridge pier with pile foundation. Nevertheless, both the structural form and water depth were clearly different from those of the complex pile-cap foundation at a water depth of 60 m investigated in this study. Liu et al. [20] conducted an underwater shaking-table test of a 1 : 100 scale pile-cap foundation using eight piles instead of all piles, the experimental results indicated that the natural frequency of the tower of cable-stayed bridge in deep-water environment was reduced by 1.7% than that without water, hydrodynamic pressure effect increased the dynamic response of the model, and its magnitude was related to structural form. Although a smaller similarity ratio was adopted in the test and the form of the simplified pile-cap foundation was relatively simple, it has certain reference significance for exploring the dynamic responses of deep-water pile-cap foundations under earthquake excitation. Previous studies mentioned above have shown that bridge pier foundation built in water responds differently than that without water under seismic excitation.

At present, pile-cap foundations are widely used in deep-water bridges [21], but the diameter of the piles is generally within 4.5 m and there are no actual engineering cases for water depths exceeding 45 m; there are limited underwater shaking-table tests of the pile-cap foundation of deep-water bridges based on a particular engineering field. Most structural models in existing tests are single and simple, and the simulated water depth is less than 45 m. There are almost no test reports that systemically investigate the effects of deep-water action on seismic responses and the distribution law of hydrodynamic pressure along the height of complex pile-cap foundation under earthquakes, particularly for complex pile-cap foundations with four or more rows of piles in deep-water environments. Moreover, almost no relevant experiments have been found to investigate the distribution law of hydrodynamic pressure on large-sized caps.

In practical projects, pile-cap foundations of deep-water bridges are mostly large in scale and typically have a relatively complex structure. As the largest span highway-railway joint bridge under construction in the world, the total length of the Xihoumen rail-cum-road bridge of the Ningbo-Zhoushan Railway is 2664 m. Fifth pile-cap foundations on the main bridge were built in a 60 m deep-water environment, as shown in Figure 1. The cap is round-ended with an overall dimension of $68 \times 46.4 \times 10$ m, the diameter of eighteen piles is 6.3 m, and it is the largest bridge grouting pile in the world. Eighteen ultra-large-diameter piles are rock-socketed piles, and there is basically no soil covering layer on the seabed. The length of eighteen piles from the seabed to the cap is 54 m. The solid concrete used for the piles and cap was C45 marine concrete with a density of $2550\ \mathrm{kg \cdot m^{-3}}$ and an elastic modulus of 3.35×10^4 MPa. The seismic-peak ground acceleration of the site was $1.352\ \mathrm{m \cdot s^{-2}}$, corresponding to a 1 : 50 year event with a probability of exceedance of 10%, based on basic ground motion data.

For the abovementioned 60 m deep-water pile-cap foundation of Xihoumen rail-cum-road bridge, pile-cap foundation with 6.3 m super-large-diameter pile is first applied to the practical engineering for water depths exceeding 60 m, and its scale and complexity are far more than previous pile-cap foundations of other sea-crossing bridges. Owing to its large dimensions, complexity, and significant three-dimensional characteristics, it is difficult to accurately simulate the dynamic response of complex deep-water pile-cap foundation under the earthquake excitation by using existing theory. In view of the research deficiency of complex pile-cap foundation in deep water, particularly for the

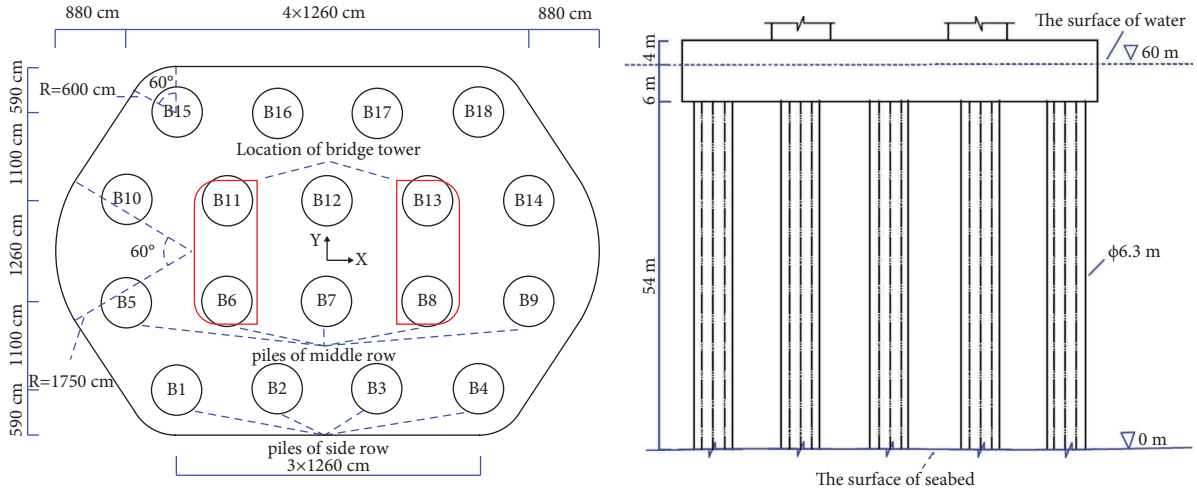

Figure 1: Layout of 60 m deep-water pile-cap foundation of Xihoumen rail-cum-road bridge.

mechanical characteristics of complex piles and the distribution law of hydrodynamic pressure on different piles and caps, the dynamic tests of complex pile-cap foundation for simulating earthquakes were conducted using underwater shaking table, the complex pile-cap foundation was designed and constructed with a scale factor of 1 : 60, and the test results are systematically summarized. Relevant research of physical modeling results not only guides the actual engineering design and construction but also provides important support for revealing the mechanical characteristics of complex pile-cap foundation and the distribution law of hydrodynamic pressure acting on piles and caps in deep-water environments.

2. Test Program

2.1. Test Equipment. In order to adopt a larger scale factor in the test, the underwater shaking-table test of a deep-water pile-cap foundation simulating an earthquake was conducted in the underwater shaking-table laboratory in Hohai University, which was currently the largest underwater shaking table in China. The maximum load-carrying capacity of underwater shaking table is 30 000 kg in the normal working range, and it can shake in X- and Y-direction with a maximum acceleration of 1.55 g and Z-direction with a maximum acceleration of 1.40 g. The length, width, and height of the test pool was 30, 20, and 1.5 m, respectively. Double-wave absorbers were set around the pool. The wide-pool and double-wave absorbers can better eliminate the boundary and reflect wave effects arising from the pool wall.

2.2. Model Design. To achieve fixation of eighteen piles and the shaking table, a 4 cm thick adapter plate was set at the bottom of the model. The full-water level was 1.22 m, and the height from the top surface of the adapter plate to the water surface (effective water depth) was 1.0 m. The actual water depth of the pile-cap foundation of Xihoumen rail-cum-road bridge is 60 m; however, owing to the limitation of 1.0 m effective water depth adopted in the test, the geometric similarity ratio of the pile-cap foundation was determined to be 1 : 60.

The dynamic scale-model test of fluid-structure coupling problems has more complex mechanical properties than ordinary dynamic tests. On the one hand, the model generates internal forces under shaking-table excitation; on the other hand, the surrounding fluid domain generates a restoring force on the model motion. Therefore, the characteristics of the structural model and fluid should be comprehensively considered when designing the structural model. According to previous studies [22, 23], the dynamic scale-model test of fluid-structure coupling problems mainly followed the structure dynamic similarity and fluid similarity criteria, which typically include Euler similarity criterion and Froude similarity criterion. According to the similarity theory and reference [22], the main similitude criteria are described in equations (1)–(3).

(1) Structure dynamic similarity criterion:

$$\frac{S_E}{S_\rho . S_a} = S_L. \tag{1}$$

(2) Froude similarity criterion:

$$\frac{S_v}{\sqrt{S_L . S_g}} = 1. \tag{2}$$

(3) Euler similarity criterion:

$$\frac{S_P}{S_\rho . S_v^2} = 1, \tag{3}$$

where M_i is the similarity ratio of the physical quantities defined as $S_i = i_{\text{mod}}/i_{pro}$. i_{mod} and i_{pro} represents the physical quantities of the test scale model and the prototype structure, respectively. The subscripts of L, E, ρ, a, v, and P represent the geometric dimensions, elastic modulus, material density, acceleration, velocity, and hydrodynamic

pressure, respectively. It is noted that the similarity ratio of the gravitational acceleration is 1.0, and the similarity ratio of the geometric dimensions is determined to be 1 : 60, which is limited by the maximum test water depth. The values of these two parameters are first determined and difficult to change.

To meet the structure dynamic similarity and fluid similarity criteria, it is assumed that there is an ideal material with an elastic modulus $E = 558.3$ MPa and a density $\rho = 2550\ \text{kg/m}^3$, that is, elastic modulus similarity ratio $S_E = 1 : 60$ and density similarity ratio $S_\rho = 1.0$. All the above similarity criteria can be well satisfied. At the same time, the material characteristics, geometric characteristics, and dynamic characteristics of the ideal material model can be determined accordingly.

In order to provide better feedback on the similarity relationship of the test model and prototype structure, Table 1 shows the similarity ratio parameters of the prototype structure and the test model using the above ideal materials.

In practice, it is difficult to obtain the abovementioned ideal materials, and it is necessary to replace piles and caps according to the available materials during the design and processing of complex pile-cap foundation models.

2.2.1. Design of Eighteen Piles. Referring to the underwater shaking test performed in previous studies of [19], piles used in this study were made of polymethyl methacrylate. To accurately obtain the dynamic elastic modulus of polymethyl methacrylate, three beams of $4 \times 4 \times 40$ cm were made of the same batch of materials. The dynamic elastic modulus of polymethyl methacrylate material was obtained by measuring the fundamental frequency of three cantilever beams. The fundamental frequency of the three cantilever beams is obtained by both sweeping resonance and hammering methods. Through mutual calibration, the dynamic elastic modulus of polymethyl methacrylate is 4.01 GPa and the density is $1198.9\ \text{kg}\cdot\text{m}^{-3}$.

For pile-cap foundation model with the ideal material, the outer diameter of piles is 105 mm, and the effective height of single pile is 0.9 m. Elastic modulus of ideal material is E_i, area moment of inertia for single pile is I_i, the effective height of the pile is L_i and its value is 0.9 m, corresponding stiffness of single pile is $(E_i.I_i/L_i)$, and its value is 3699.4 N·m. On the premise of maintaining the overall layout of eighteen piles, the overall dimensions and stiffness of each pile were unchanged, and polymethyl methacrylate was used to reasonably replace the above ideal materials of eighteen piles. It was determined that the eighteen piles can be made of hollow polymethyl methacrylate pipes; the outer diameter of the hollow pipe was 105 mm, the inner diameter was 101 mm, and the thickness was 2 mm. Elastic modulus of polymethyl methacrylate is E_p, area moment of inertia for single pile is I_p, the effective height of single pile is L_p and its value is 0.9 m, corresponding stiffness of single pile is $(E_p.I_p/L_p)$ and its value is 3783.4 N·m, which is close to 3699.4 N·m, and the difference of stiffness between ideal material pile and polymethyl methacrylate pile is 2.3%.

The effective height of single pile is 0.9 m, and the mass of ideal material pile and polymethyl methacrylate pile is 19.9 kg and 0.7 kg, respectively. To compensate for the difference in mass density to satisfy the similarity relationship of material density, the counterweight should be uniformly increased from bottom to top in hollow polymethyl methacrylate pipes. To avoid affecting the stiffness of the piles and reduce the influence of the shaking impact on the test results, nine hollow cylindrical steel blocks were placed in the middle of each pipe. The diameter of each block was 7 cm and the height was 10 cm, and the remaining gap was filled with prepared steel sand. Each hollow pipe was filled with 19.2 kg of counterweight, and the total weight of the eighteen pipes was 345.6 kg; through the design of counterweight, the ideal material piles and polymethyl methacrylate piles have the same mass.

The elastic modulus of polymethyl methacrylate is about seven times that of ideal material. Through the above design of equivalent stiffness replacement by using hollow piles, the same position of ideal material pile and polymethyl methacrylate pile still has the same strain, acceleration, and displacement. The new model still meets the structure dynamic similarity criteria and fluid similarity criteria of the dynamic scale-model test of fluid-structure coupling problems.

2.2.2. Design of Round-Ended Cap. As the cap of the prototype structure is a large reinforced-concrete structure, it can be regarded as a rigid body whose deformation is far less than the displacement [24–26], the overall dimension of the model cap is $113.3 \times 77.3 \times 16.7$ cm, and the cap mass of the test model is 320.0 kg. On the premise of ensuring the same mass and overall dimension of round-ended cap, whether using ideal material or other alternative materials can guarantee that the model design still meets the similarity relationship. Because the steel cap is easier to control its total mass and irregular shape, steel cap with same mass and size is used in the test instead of the ideal material cap, and it still can be regarded as a rigid body. Seven small grooves have been reserved in the designated position for installing hydrodynamic-pressure sensors.

2.2.3. The Connection of Complex Model. To achieve the arrangement of the signal wires from the sensors and realize the rigidity connection between the bottom of the cap and the top of eighteen piles, there are eighteen reserved holes evenly arranged at the cap according to the position of the eighteen piles. In order to realize the fixed boundary connection between piles and the cap, according to the mass requirements of the excavated cap, the upper diameter of 18 reserved holes is 8 cm and corresponding height is 10.67 cm, and the lower diameter is 11.3 cm and corresponding height is 6.0 cm, such that the top of eighteen piles can extend into the cap for 6 cm. The gap between the outer side of the pile top and the cap is about 0.4 cm, the upper surface of the pile top is in contact with the cap, and the contact surface and the

Table 1: Similarity ratio parameter.

Type	Physical variables	Similarity relation
Material properties	Stress	$S_\sigma = S_E = 1/60$
	Strain	$S_S = 1$
	Elastic modulus	$S_E = S_E = 1/60$
	Density	$S_\rho = 1.0$
Geometric characteristics	Length/width/height	$S_L = 1/60$
	Area	$S_A = S_L^2 = 1/3600$
	Displacement	$S_w = S_L = 1/60$
Dynamic characteristics	Quality	$S_m = S_\rho S_L^3 = 1/216000$
	Stiffness	$S_k = S_E.S_L = 1/3600$
	Time	$S_t = S_L^{0.5} = 1/7.75$
	Frequency	$S_f = S_L^{-0.5} = 7.75$
	Acceleration	$S_a = 1$
	Gravitational acceleration	$S_g = 1$
	Velocity	$S_v = S_L^{0.5} = 1/7.75$

tiny gap are firmly connected with the structural adhesive, which is mainly composed of epoxy resin, etc. Eighteen piles and the cap are connected in the same way, and the piles and the cap can be considered as a fixed boundary condition.

The connection of the piles and the adapter plate is similar to the fixed connection of eighteen piles and the cap. The reserved hole diameter of adapter plate is 11.3 cm, which is larger than the outer diameter of the piles. The gap between the outer surface of pile bottom and the adapter plate is about 0.4 cm, and the bottom of the eighteen piles can extend into the adapter plate for 3.6 cm. The remaining 0.4 cm adapter plate is mainly used to bear the weight of counterweight and prevent the outflow of steel sands. The bottom surface of the piles is in contact with the adapter plate. Both the contact surface and the tiny gap are firmly connected with structural adhesive, and the pile and the cap can be considered as a fixed boundary condition. In order to simulate the anchoring boundary between rock-socketed pile and rocks, the adapter plate is connected to the shaking table with 6 bolts, which can also be seen as a fixed boundary condition. Figures 2 and 3 present the connection diagram of the pile, cap, and adapter plate. After the completion of all tests, the connections between eighteen piles and the cap and the adapter plate are still firm without looseness.

2.3. Layout of Measuring Points. The pile-cap foundation is symmetrical along the X- and Y-directions, with the sensor layout shown in Figures4 and 5. The DEWE2-M18 dynamic data-acquisition system of Dewetron GmbH, Austria, was used in this test. In Figure 4, measuring points L1 and L2 are laser-displacement sensors, which are used to measure the displacement of the model top in the X- and Y-directions. AX1–AX5 and AY1–AY3 are eight underwater acceleration sensors, AX1/AX2 is used to monitor the X-direction acceleration at the top of the shaking table and adapter plate, and AY1/AY2 is used to monitor the Y-direction acceleration at the top of the shaking table and adapter plate. In Figure 6, measuring points S1 to S33 are strain gauges, measuring points S1 to S27 are arranged at the bottom of piles, S1/S28/S29 is arranged on pile B1, S9/S30/S31 is arranged on pile B5, and S18/S32/S33 is arranged on pile B9, with heights of 2 cm, 45 cm, and 80 cm from the top of the adapter plate.

In Figure 5, P1–P20 are the integrated hydrodynamic-pressure sensors. To avoid the influence of the shaking table and adapter plate on the bottom water, the layout of the hydrodynamic-pressure sensors was started at a height of 16.7 cm. The height of P1, P4, P8, and P11 from the top surface of the adapter plate was 16.7 cm, the height of P2, P5, P7, P9, and P12 was 45 cm, and the height of P3, P6, P10, and P13 was 83.3 cm. P14–P20 were arranged at the cap with a height of 4 cm from the bottom of the cap and were used to study the distribution law of hydrodynamic pressure on a round-ended cap under earthquake excitation.

To reduce the influence of sensors and signal wires on the flow field around the pile-cap foundation model, micro-sized sensors and thin signal wires were used in an underwater shaking table. Hydrodynamic-pressure gauges were placed in the designated positions of the piles and cap through a 1 cm reserved hole, and the tiny gap between the sensors and the piles was filled with sealant to achieve waterproofing. The signal wire extends from the interior of the piles and the steel cap to the top of the model, all of which are led to the pool side along the wire rope suspended in the air and then connected to the acquisition instrument. The signal wires of the strain gauges and acceleration sensors at the bottom of the model are fixed to the top of the shaking table, and only a few thin signal wires are arranged along the pile shafts. Those signal wires are led to the pool boundary along the pool bottom, and there is basically no interference to the flow field. A panoramic view of the test site is shown in Figure 7.

2.4. Loading Conditions. The duration time of actual seismic waves generally does not exceed 60 seconds, since the time step must be compressed according to the time scale $\lambda_T = 1/7.75$. The duration time of input seismic waves in underwater shaking-table test is only a few seconds, which is closer to the pulse load rather than the seismic load. Moreover, seismic waves with too short duration do not meet research standards. Therefore, two artificial waves are input along the X-

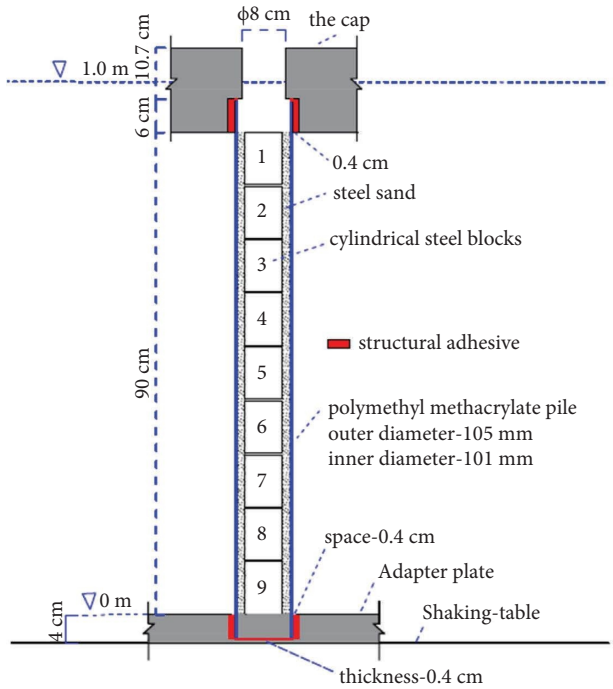

Figure 2: Connection diagram of the pile, cap, and adapter plate.

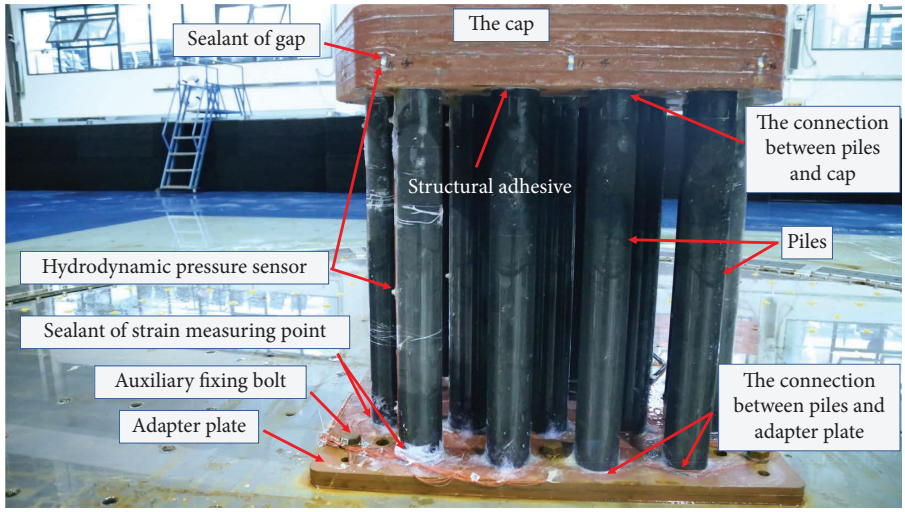

Figure 3: Structural connection display of pile-cap foundation model.

and Y-directions in this test. Based on the geological conditions of the deep-water pile-cap foundation of the Ningbo-Zhoushan Railway, the specification spectrum is determined according to Specifications for Seismic Design of Highway Bridges (JTGT2231-01-2020) [27]. Thereafter, two artificially synthesized waves were generated according to the specification spectrum of basic ground motion data, and the seismic-peak acceleration was 1.352 $m \cdot s^{-2}$. In order to avoid short loading times of seismic waves, the time of two artificial waves without time compression was set to 93 s, while the loading-wave time was set to 12 s. The acceleration-time curve of artificial wave 1 without time compression is shown in Figure 8, and the acceleration response spectrum is shown in Figure 9.

The effective water depth of underwater shaking table is 0.0 m (no water), 0.5 m, and 1.0 m. The loading conditions are presented in Table 2.

3. Test Results and Analysis

3.1. Description of the Phenomenon. Before the seismic wave excitation, the pile-cap foundation model is in the static water. Three wave-height meters are used to monitor the height change of water surface wave during the test, wave-

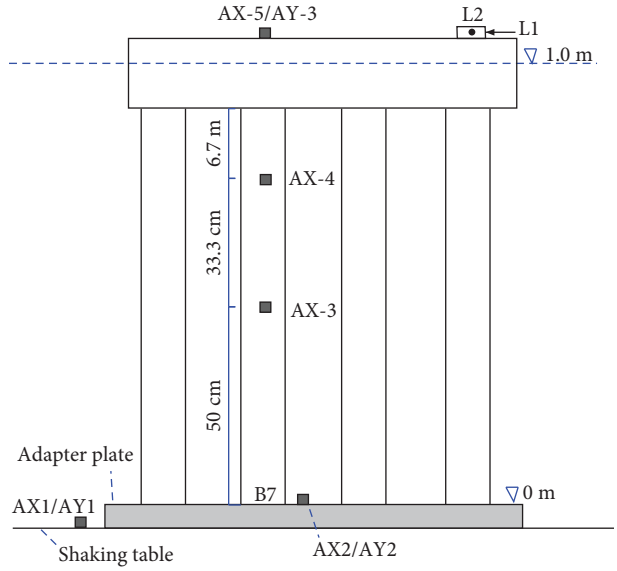

Figure 4: Layout of acceleration and displacement measuring points.

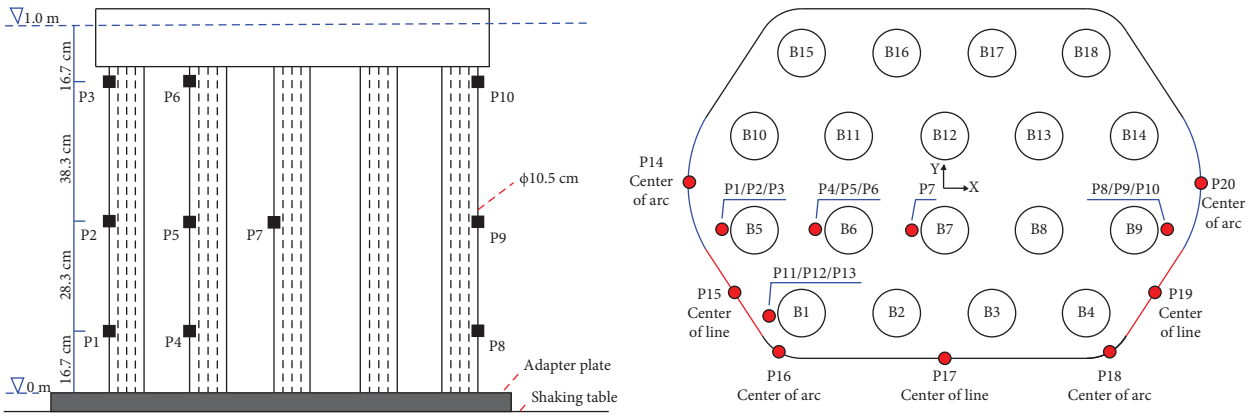

Figure 5: Hydrodynamic-pressure measuring point layout at the cap and piles.

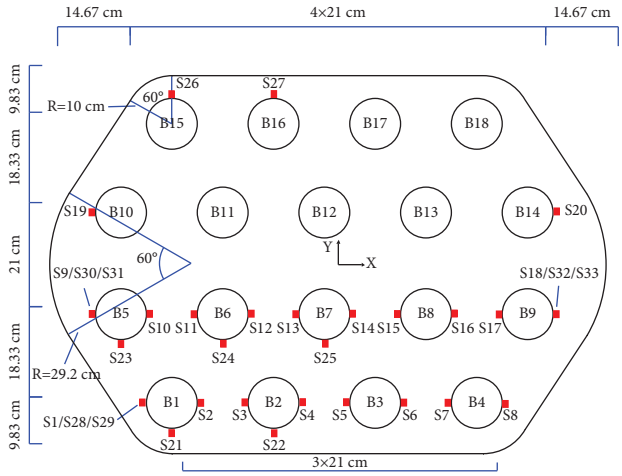

Figure 6: Layout of strain measuring points.

Figure 7: Panoramic view of test site.

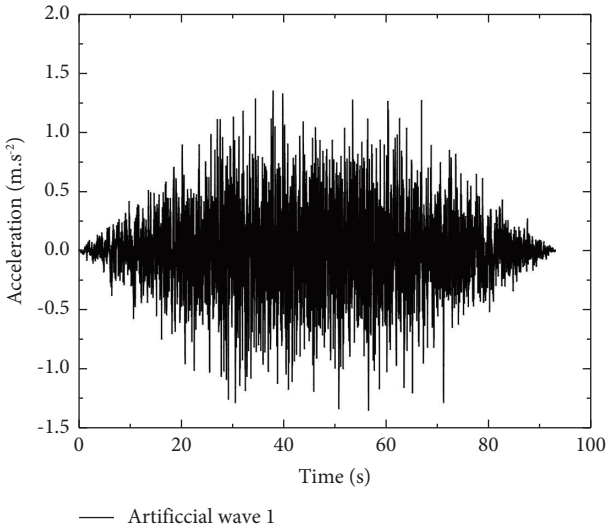

Figure 8: Acceleration-time curve of artificial wave 1.

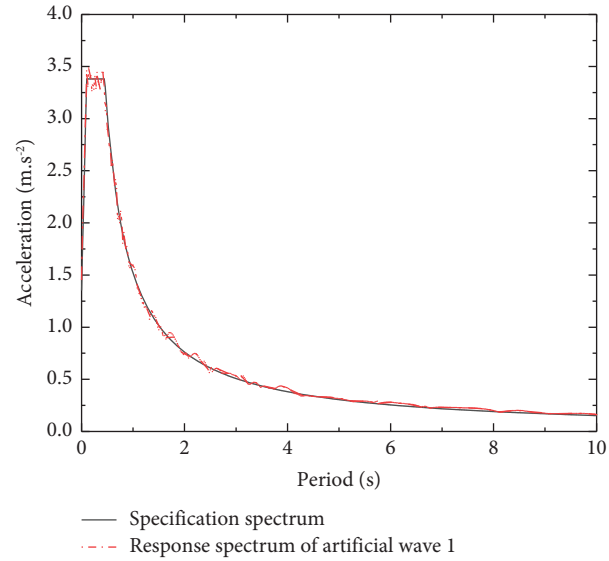

Figure 9: Comparison of acceleration response spectrum and specification spectrum.

height meter 1 is arranged in the X-direction of the model motion, and the distance is 1.5 m from the edge of the cap. Wave-height meters 2 and 3 are arranged at the pool boundary and the distance is 1.0 m from double-wave absorbers of the pool boundary, and wave-height meter 2 is perpendicular to the X-direction of the model motion, whereas wave-height meter 3 is parallel to the X-direction of the model motion. Those wave-height meters are also used as a judging rule to determine whether the water surface is in static state. The macroscopic phenomena of underwater shaking-table test are as follows.

(1) As the motion of the model, radial surface waves are generated from the center position where the model is located due to the dynamic interaction between pile-cap foundation model and the surrounding water. When the motion of the model stops, the surface waves disappear quickly. It indicates that the fluctuation of the water surface is caused by the motion of the model. When an earthquake occurs, the excitation of seismic wave can cause the motion of pile-cap foundation in water, which would disturb the water body and cause the fluctuation of the water surface. Earthquake load is a reciprocating load and the disturbed water body would act on the model structure in turn, which leads to the pier-water interaction.

(2) When artificial wave 1 and artificial wave 2 are excited along the X-direction, water surface waves mainly occur within 5 m of the model, and there is no obvious disturbance on the water surface away from 5 m. According to the displacement similarity ratio 1/60 and time similarity ratio 1/7.75, the displacement of the model is millimeter level, the duration time of the input seismic waves is 12 s, the water surface fluctuation caused by structure-water interaction is also millimeter level, and the scope of disturbance to water body is relatively limited. When artificial waves 1 and 2 are excited along the X-direction, the maximum wave height of wave-height meter 1 is 2.14 mm and 2.47 mm, the maximum wave height of wave-height meters 2 and 3 is less than 0.09 mm, and the wave height near the pool boundary is basically unchanged, which indicates that the water body at the pool boundary is basically undisturbed, and the wave-height monitoring results

Table 2: Test conditions.

Serial number	Loading wave	Water depth (m)	Acceleration peak ($m \cdot s^{-2}$)	Excitation direction
1	Artificial wave 1/artificial wave 2	0	1.352	X/Y
2	Artificial wave 1	0.5	1.352	X
3	Artificial wave 1/artificial wave 2	1.0	1.352	X/Y

are consistent with the macroscopic phenomenon of water surface.

The length, width, and height of the test pool were 30, 20, and 1.5 m, respectively, double-wave absorbers were set around the pool boundary, the distance between the pool boundary and the edge of the model is more than 9 m, sufficient water area of test pool is one major advantage of this test, the water pool can well simulate the infinite water area, and the water pool boundary effect has no interference effect on surface wave.

3.2. Influence of Water Depth on Dynamic Response of Pile-Cap Foundation Model

3.2.1. Analysis of Water Depth Influence on Natural Vibration Period. The natural vibration period of complex pile-cap foundation model is identified through white noise tests of different water depths, Table 3 shows the natural vibration period of the complex pile-cap foundation model in different water depths. The natural vibration period of the test model was 0.1148 s under the waterless condition, 0.1172 s for a 0.5 m water depth, and 0.1212 s for a 1.0 m water depth, respectively. Compared with the waterless condition, the increase rates were 2.1% and 5.6%, respectively, the increase rate of natural vibration period in 1 m water depth is 2.7 times that of 0.5 m water depth, and the corresponding ratio is greater than water depth ratio of 2.0, which indicates that the existence of water can prolong the natural vibration period of complex pile-cap foundation, while the increase in natural vibration period is non-linear related to water depths.

At present, the theory of hydrodynamic pressure was mainly about single pier structures, the relevant theoretical explanation of hydrodynamic pressure for complex pile-cap foundations under earthquake action has not yet been well understood [28, 29], and the main reason was that the surrounding piles can influence the hydrodynamic pressure of a certain pile and the influence varies with different factors such as the arrangement and spacing distance. According to the contribution of Liaw and Chopra [30] and Li and Yang [31] for single cylindrical piers, the dynamic equilibrium equation of the submerged cylindrical pier under seismic excitations can be simplified as follows:

$$[M + M_w].\ddot{x} + C.\dot{x} + K.x = (M + M_w)\ddot{x}_g, \quad (4)$$

where M, C, and K represent structural mass, damping, and stiffness matrices, respectively; $\ddot{x}$, $\dot{x}$, and x represent cylinder acceleration, velocity, and displacement, respectively; and $\ddot{x}_g$ is acceleration of the ground.

Although there are some assumptions and simplified processing methods that differ from the actual situation, equation (4) developed a method to transform the hydrodynamic forces during an earthquake into a hydrodynamic added mass, which is meaningful for theoretical exploration. Although differing from vibration of traditional single pile, the existence of adjacent piles changes the distribution of hydrodynamic pressure on each pile of pile-cap foundation, and water body has the same influential mechanism on single pier or complex pile-cap foundation.

Table 3: Natural vibration period of complex pile-cap foundation model.

Number	Water depth (m)	Natural vibration period (s)	Var R (%)
1	0	$T_1 = 0.1148$	—
2	0.5	$T_2 = 0.1172$	2.1
3	1.0	$T_3 = 0.1212$	5.6

Var R is defined as follows: $R = (T_i - T_1/T_1) \times 100\%$, where T_i and T_1 represent the natural vibration period of pile-cap foundation model in water and without water, respectively.

The added mass theory of the hydrodynamic forces mentioned above can be used to explain the variation of the natural vibration period of pile-cap foundation model in different water depths. The added mass is dependent on water depths, a higher water depth causes a larger added mass, resulting in an increase in the natural vibration period, and the tendency in theoretical analysis is consistent with the conclusion obtained from experimental investigation results of natural vibration period.

3.2.2. Analysis of Water Depth Influence on Acceleration. Artificial wave 1 is excited along the X-direction under three different water depths of 0.0 m, 0.5 m, and 1.0 m. The maximum acceleration of measuring points AX3, AX4, and AX5 is divided by the maximum acceleration of measuring point AX2, which is on the top surface of the adapter plate. The normalized acceleration-amplification coefficient of the model is obtained, and the corresponding value is shown in Figure 10. The distribution of the acceleration-amplification coefficient in the model did not show a consistent increasing trend from bottom to top. Compared with the values on the bottom and top of the model, the acceleration-amplification coefficient of measuring point AX3 in the middle of pile B7 is significantly larger, which is related to the complex structural form of the pile-cap foundation. Due to the large diameter and large number of piles, the volume and mass of the cap are huge, and the cap motion will produce great horizontal inertia force under earthquake excitation because their high-rise pile caps are top-heavy. The piles between the adapter plate and the cap have no lateral restraint; meanwhile, the cap and 18 piles are rigidly connected, and the coupling effect of the piles and the cap will restrict the top

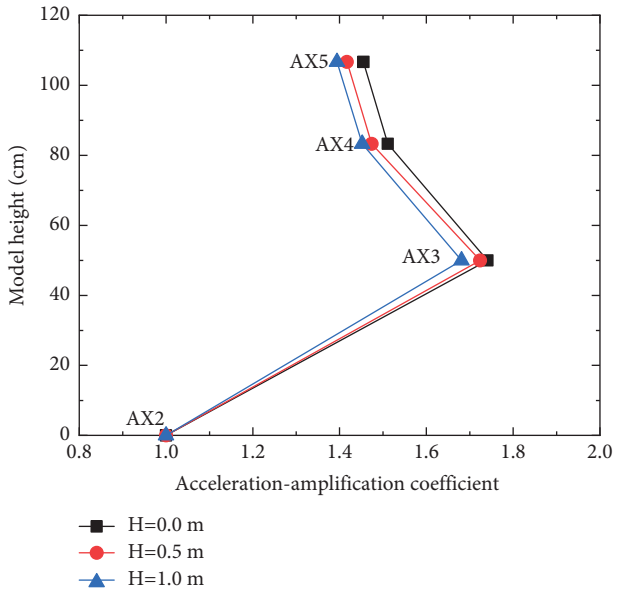

Figure 10: Variation in acceleration-amplification coefficient along model height.

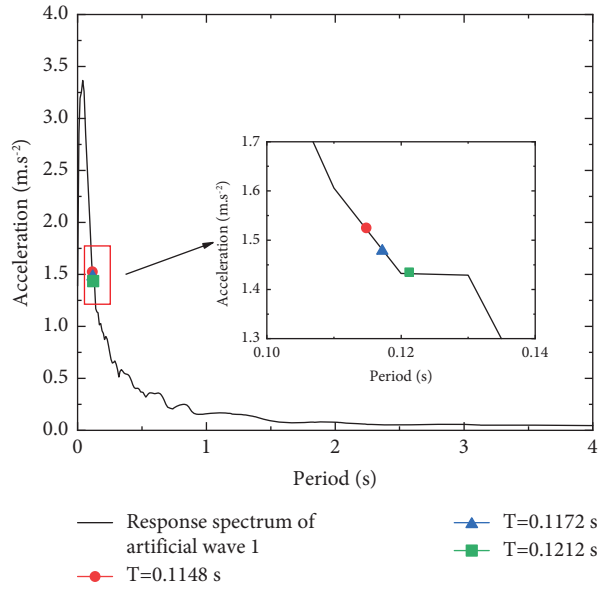

Figure 11: Acceleration response spectrum of input seismic wave.

motion of eighteen piles along the seismic direction, which will significantly change the internal force and acceleration distribution of the piles. Compared to the excitation of artificial wave 1 under the waterless conditions, the acceleration-amplification coefficient of the same position shows a decreasing trend under 0.5 m and 1.0 m water depth. The acceleration of measuring point AX5 at the model top decreases by 2.6% and 4.2%. Previous studies of reference [17] have shown that the presence of water significantly increases the acceleration of pier top because the water around the pier increases added inertial forces of the pier under earthquake. However, the results in this study obtained the opposite conclusion; when considering the water effect, the seismic acceleration of complex pile-cap foundation model decreased. The main reason for this experimental phenomenon is that the acceleration response of complex pile-cap foundation model in water is not only increased by the hydrodynamic pressure resulting from water-pier interaction but also decreased by the damping forces of the water body, and the effect of the damping forces has a larger influence on acceleration than that of hydrodynamic pressure, so the acceleration responses of complex pile-cap foundation model measured from the underwater shaking-table test decrease.

The influence of water depths on acceleration response of complex pile-cap foundation model can also be explained based on the spectral characteristics of artificial seismic waves. Through underwater acceleration sensor AX2, the actual acceleration-time curve of input seismic wave can be obtained, the acceleration response spectrum of artificial wave 1 is shown in Figure 11, and the local enlarged drawing highlights the change of the natural vibration period in three different water depths. It is evident that the amplitude of the acceleration response spectrum decreases with the increase of the period, which shows that the acceleration-amplification coefficient will theoretically decrease in a higher water depth, and the test result is in accordance with the theoretical analysis of the acceleration response spectrum. From the experimental results and the above analysis, it can be concluded that the existence of water can prolong the natural vibration period of pile-cap foundation; meanwhile, the influence of the water depths on the acceleration depends on the acceleration response spectrum of the input seismic wave.

3.2.3. Analysis of Water Depth Influence on Pile Strain. Artificial wave 1 was excited along the X-direction when the water depth was 0.0 m, 0.5 m, and 1.0 m. The maximum tensile strain of the pile-cap foundation model occurred at strain measuring point S9, which is at the bottom of pile B5. Figure 12 presents a comparison of the maximum tensile strain of pile B5 along the model height. The maximum tensile strain of pile B5 decreases first and then increases from bottom to top, the tensile strain value of the measuring point S9 is obviously larger than that of S30 and S31, and the strain distribution of pile B5 under three different water depths is similar, so the bottom of complex pile-cap foundation was most likely to be damaged first under earthquake action, which demonstrates that the bottom of the pile is the key control section and the weak point of complex pile-cap foundation. With an increase in water depth, the maximum tensile strain at measuring points S9, S30, and S31 of pile B5 showed an increasing trend, which indicates that the hydrodynamic pressure on complex pile-cap foundation increases the strains of the piles, and the maximum strain of the pile-cap foundation increased significantly with an increase in water depth.

When the water depth is 0.0 m and 1.0 m, the strain-time curve of measuring point S9 at the bottom of pile B5 is

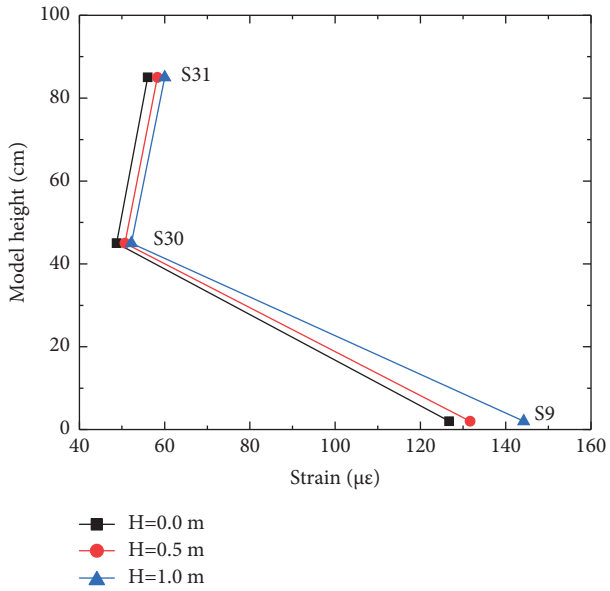

Figure 12: Variation in maximum strain along the height of pile model subjected to different water depths.

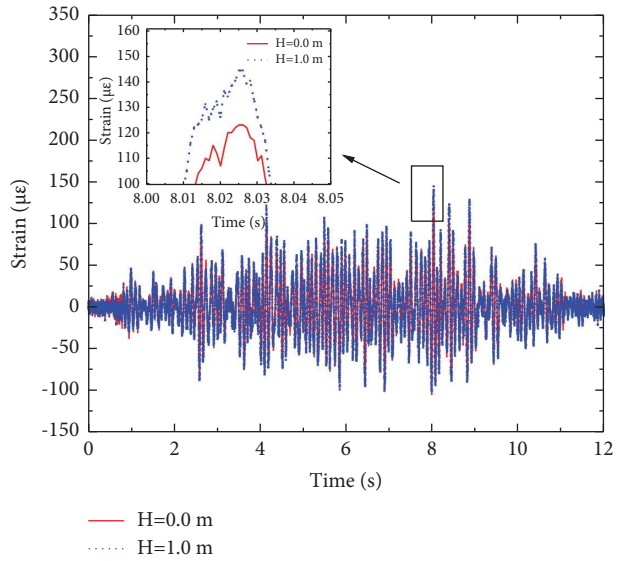

Figure 13: Strain-time curve of measuring point S9 subjected to different water depths.

shown in Figure 13. The trend of strain-time curve in 1.0 m water depth is similar to that of the waterless condition; because of hydrodynamic pressure effect, the water body can affect the dynamic response of the model strain, the hydrodynamic force is significantly less than the structural force, and variation trends of the dynamic response in 1.0 m water depth are still similar to waterless condition, but the dynamic response peak is significantly different. The maximum tensile strain of measuring point S9 was 126.7 $\mu\varepsilon$ when the water depth was 0.0 m, and the strain value of S9 was 131.7 $\mu\varepsilon$ and 144.2 $\mu\varepsilon$ when the water depth was 0.5 m and 1.0 m, respectively. Compared with the waterless condition, the maximum tensile strain increment was 5.0 $\mu\varepsilon$ for 0.5 m water depth and 17.5 $\mu\varepsilon$ for 1.0 m water depth, and the increase rates were 3.9% and 13.8%, respectively. It is obvious that a higher water depth results in a considerably larger strain. The strain at the bottom measuring point S9 of the pile B5 increases much faster with increasing water depth. The reasons for the above phenomena are as follows: the seismic excitation will cause the motion of the pile-cap foundation model in water, the relative motion of the model and the surrounding water body will generate the hydrodynamic added mass induced to the hydrodynamic pressure, and the hydrodynamic added mass increases the additional inertial forces on the pile-cap foundation model, which has a large bending moment on the bottom of the piles resulting in a larger strain at the bottom in comparison with the upper positions of the piles.

Artificial wave 1 is excited along the Y-direction when the water depth was 0.0 m and 1.0 m, and the maximum tensile strain was 128.8 $\mu\varepsilon$ and 148.2 $\mu\varepsilon$, respectively, and occurred at measuring point S21, which is at the bottom of pile B1. Compared to the waterless condition, the maximum tensile strain increment was 19.4 $\mu\varepsilon$ for 1.0 m water depth and the increase rate was 15.1%. In conclusion, when artificial wave 1 was excited along the X- or Y-directions, the strain of deep-water pile-cap foundation was greater than that without water, which indicated that the influence of hydrodynamic pressure should be considered in the seismic design of complex deep-water pile-cap foundation.

Artificial wave 1 was excited along the X- and Y-directions when the water depth was 0.0 m, and the maximum tensile strain of pile-cap foundation model was 126.7 $\mu\varepsilon$ and 128.8 $\mu\varepsilon$ and the value of the latter was 101.7% of the former. Artificial wave 1 was excited along the X- and Y-directions when the water depth was 1.0 m, and the maximum tensile strain of pile-cap foundation was 144.2 $\mu\varepsilon$ and 148.2 $\mu\varepsilon$, the value of latter being 102.8% of the former. Whether subjected to 0.0 m or 1.0 m water depth, the maximum tensile strain of pile-cap foundation model under X- and Y-direction excitation was relatively close, and the overall difference was within 3%. For complex pile-cap foundation used in Xihoumen rail-cum-road bridge, the layout of eighteen ultra-large-diameter piles can provide a meaningful reference for seismic design of deep-water pile-cap foundation of other cross-sea bridges.

3.2.4. Analysis of Water Depth Influence on Model Top Displacement. Artificial wave 1 was excited along the X-direction under 0.0 m and 1.0 m water depths, and the displacement-time curve of the model top is shown in Figure 14. The maximum displacement was 2.074 mm when the water depth was 0.0 m, and its values were 2.101 mm and 2.155 mm when the water depth was 0.5 m and 1.0 m, respectively. Compared with the waterless condition, the maximum displacement increment was 0.027 mm for 0.5 m water depth and 0.081 mm for 1.0 m water depth; the increase rates were 1.3% and 3.9%, respectively.

At present, it was very difficult to measure the bottom displacement of model piles in water, the shaking table was a huge rigid body, and its motion characteristics were

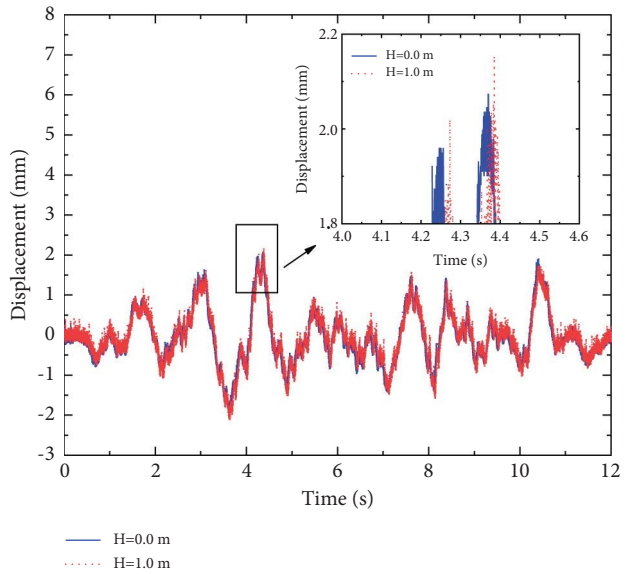

Figure 14: Displacement-time curve of model top subjected to different water depths.

basically consistent with the dynamic response of the pile bottom, so the displacement of the shaking table can be regarded as the bottom displacement of pile-cap foundation model and its value was equal to the rigid body displacement of the model caused by the seismic wave. When artificial wave 1 was excited along the X-direction, the maximum rigid body displacement of pile-cap foundation model was 1.917 mm according to the feedback data of shaking-table sensor. When the water depth was 0 m, 0.5 m, and 1.0 m, the maximum rigid body displacement was 92.4%, 91.2%, and 89.0% of the maximum top displacement, respectively, which indicates that the value of the measured displacement of cap top was primarily that of a rigid-body displacement, the motion of the pile-cap foundation model under earthquake excitation is similar to that of rigid bodies, and this phenomenon is mainly caused by the high stiffness of the pile-cap foundation.

The maximum displacement increment caused by 0.5 m water depth was 0.027 mm, and the corresponding values were 1.4% of rigid-body displacement and 1.3% of the total displacement. The maximum displacement increment caused by 1.0 m water depth was 0.081 mm, and the corresponding values were 4.2% of rigid-body displacement and 3.9% of the total displacement. The displacement increment subjected to 1.0 m water depth influence was basically 3.0 times that of 0.5 m water depth, and the ratio was far greater than water depth ratio 2.0, which indicates that the increase of model displacement was non-linear related to the water depth. Although the displacement increment caused by the water influence accounts for a small proportion of the total displacement, the displacement increment change trend can still reflect the water-depth change influence trend of the top displacement of the pile-cap foundation, and the displacement of complex pile-cap foundation model measured from the underwater shaking-table test increased with increasing water depths. When considering the water influence, the top displacement of complex pile-cap foundation model is decreased by the damping forces resulting from the water but also increased by the added mass induced to the hydrodynamic pressure, and the final trend of displacement response is the comprehensive result of two effects. The influence of hydrodynamic pressure on the top displacement is greater than that of the damping forces, so the top displacement of complex pile-cap foundation measured from the test increases with the increase of water depths.

3.3. Hydrodynamic-Pressure Analysis of Complex Pile-Cap Foundation Model

3.3.1. Influence of Water Depth on Hydrodynamic Pressure. The measuring points P11 of pile B1, P1 of pile B5, P4 of pile B6, and P8 of pile B9 were arranged at 16.7 cm from the top surface of the adapter plate. When the water depth was 0.5 m and 1.0 m, four measuring points were all below the water surface. When artificial wave 1 was excited along the X-direction, maximum hydrodynamic pressure of four measuring points under 0.5 m and 1.0 m water depth occurred and is shown in Figure 15. Compared with the 0.5 m water depth, the hydrodynamic pressure at the same location at 1.0 m water depth was significantly greater. The maximum hydrodynamic pressures at measuring points P11, P1, P4, and P8 under a 0.5 m water depth are 80.8%, 77.8%, 85.1%, and 74.1% of the value under 1.0 m water depth, respectively, and the corresponding ratio is between 74.1% and 85.1%. The test results of different water depths show that the hydrodynamic pressure at the pile bottom increases with the increment of water depth. According to the acceleration test results in Section 3.2.2, when the water depth was 0.5 m and 1.0 m, the difference of model acceleration was basically within the range of 2.5%, which indicated that the dynamic response of the model was not the main reason for the significant difference of hydrodynamic pressure in different water depths. The influencing mechanisms for the above phenomena are as follows: the actual water body is compressible; meanwhile, the motion of the model under earthquake excitation will cause water surface waves. There is a boundary condition that the hydrodynamic pressure value is 0 Pa on the water surface, and those factors would affect the hydrodynamic pressure attenuation, and the attenuation influence of hydrodynamic pressure increases with the decrease of the distance from the water surface. It is evident that a lower water depth results in a closer distance from the measuring point to the water surface, so the hydrodynamic pressure of the same location at 0.5 m water depth is significantly smaller than that of 1.0 m water depth.

The measuring points P12 of pile B1, P2 of pile B5, P5 of pile B6, and P9 of pile B9 were arranged at 45.0 cm from the top surface of the adapter plate. When the water depth was 0.5 m, four measuring points were all below the water surface and the distance from the water surface is 5.0 cm, while the distance of four measuring points from the water surface is 55.0 cm when the water depth was 1.0 m. To further investigate the impact of water depth on hydrodynamic

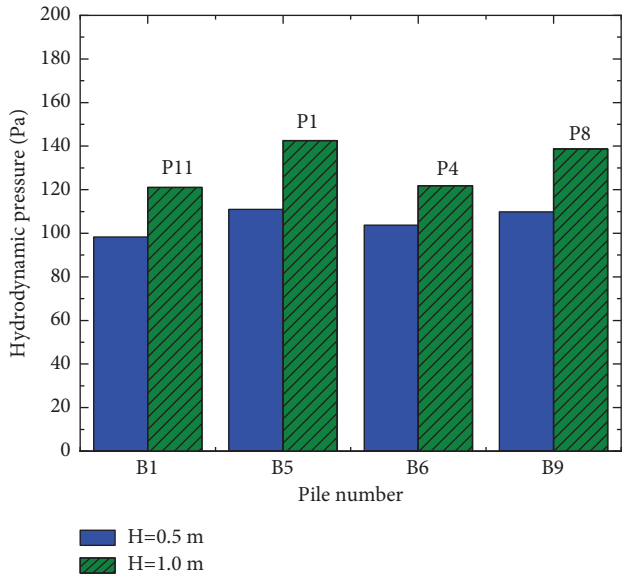

Figure 15: Variation in hydrodynamic pressure under different water depths.

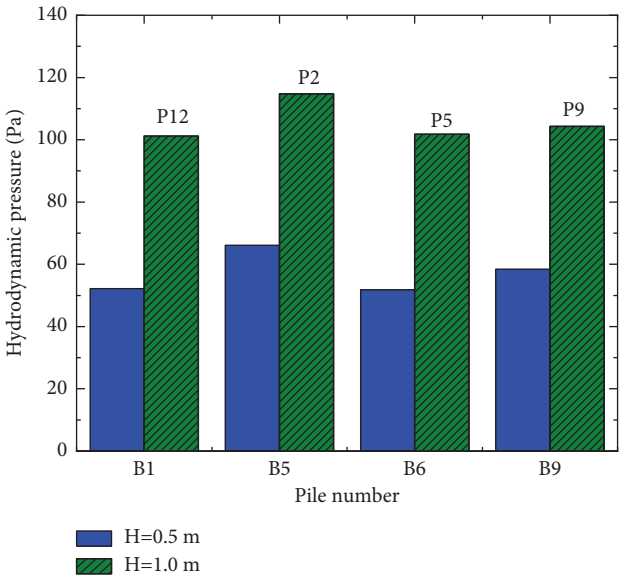

Figure 16: Variation in hydrodynamic pressure under different water depths.

pressure, for 0.5 m and 1.0 m water depth, the comparison of the maximum hydrodynamic pressure for abovementioned measuring point is shown in Figure 16. Compared with the 0.5 m water depth, the hydrodynamic pressure at the same location at 1.0 m water depth was significantly greater. The maximum hydrodynamic pressures at measuring points P12, P2, P5, and P9 under a 0.5 m water depth are 51.6%, 57.6%, 50.9%, and 56.0% of the value under 1.0 m water depth, respectively, and the corresponding ratio is between 50.9% and 57.6%; there is a more significant difference in hydrodynamic pressure at this height. For these measuring points of hydrodynamic pressure, the water depth and distance from the water surface are the main differences, which indicate that the hydrodynamic pressure is closely related to the water depth, and the attenuation effect significantly increases with the decrease of the distance from the water surface. These observations are in accordance with the results of theoretic analysis.

3.3.2. Hydrodynamic-Pressure Analysis of Different Piles. For 1.0 m water depth, the distribution of the maximum hydrodynamic pressure on edge piles B5 and B9 and the round-ended cap along the model height is shown in Figure 17. The hydrodynamic pressure acting on each pile gradually decreased from bottom to top, while there was a sudden increasing trend at measuring points P14 and P20 of the round-ended cap. The hydrodynamic pressure under earthquake is caused by the motion of the structure, and the Morison equation shows that the earthquake-induced hydrodynamic pressure depends on water depth, diameter and acceleration of the structure, and inertial coefficient. Due to the existence of large-sized cap, the model shape at the cap position increased suddenly, part of the large-sized cap was in contact with water and changed the distribution laws of hydrodynamic pressure, which indicates that the

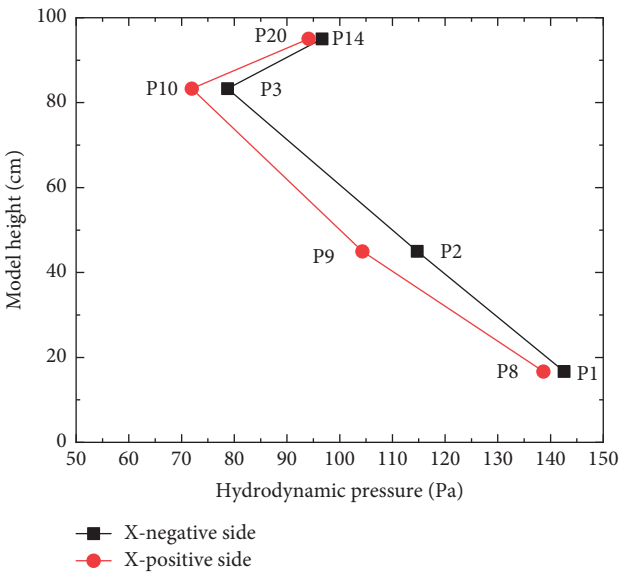

Figure 17: Variation in hydrodynamic pressure along model height.

hydrodynamic pressure was related not only to the water depth but also to the actual engineering structure. From Figure 17, it can be seen that the distribution laws of hydrodynamic pressure on both sides of the pile-cap foundation model along the model height were consistent, and the values of measurement points at the same height were also relatively close, and this is mainly because seismic load is a reciprocating load, so the hydrodynamic pressure on positive side and negative surface is highly similar, and the distribution characteristics of hydrodynamic pressure on deep-water bridge piers are significantly different from hydraulic structures such as dams.

According to the results of strain analysis in Section 3.2.3, the maximum tensile strain increment was 5.0 $\mu\varepsilon$ for 0.5 m water depth and 17.5 $\mu\varepsilon$ for 1.0 m depth water, the strain increment subjected to 1.0 m water depth influence is basically 3.5 times that of 0.5 m water depth, and the ratio is far greater than the water depth ratio 2.0, which indicates that the strain increment of the pile-cap foundation model is non-linear to the water depths. Hydrodynamic pressure effect is the main reason for the increase of pile strain, and the variation in hydrodynamic pressure in Figures 15 and 16 indicates that the hydrodynamic pressure was related to the water depth; when the water depth is 1.0 m, the hydrodynamic pressure at the same position of the piles is greater than that of 0.5 m water depth, which is one reason for larger strain increment. The variation of Figure 17 indicates that hydrodynamic pressure has a sudden increasing trend at the cap, the size of round-ended cap is much larger than that of the piles, it has larger contact area with the surrounding water, and special geometric characteristic easily leads to better blocking effect. The interaction between the large-sized cap and water is more direct and it will make the model bear greater hydrodynamic force, which is another important reason for the significant increase of pile strain in 1.0 m water depth.

Measuring point P11 was on edge pile B1 of the side-row piles, and measuring point P1 was on edge pile B5 of the middle-row piles. When the water depth was 0.5 m and 1.0 m, the hydrodynamic pressure at measuring point P11 was 88.7% and 84.9% of that of measuring point P1, respectively. The hydrodynamic pressure on pile B5 was significantly larger under X-direction excitation, mainly because pile B5 was the front-row pile, and its position was closer to the seismic excitation center. The small spacing of adjacent piles B1, B10, and B5 perpendicular to the excitation direction can easily lead to an interference effect, and the motion state of the fluid particle changed when the surrounding water passed through pile B5, which increased the hydrodynamic pressure acting on pile B5.

Figure 18 shows the maximum hydrodynamic pressure of piles B5 and B6 along the model height. Viewed from the X-direction, pile B5 is an edge pile, whereas pile B6 is a secondary edge pile. The hydrodynamic pressure on the secondary edge pile B6 was evidently less than that on pile B5, and the hydrodynamic pressure at the three measuring points on pile B6 was 85.4–88.9% of the corresponding measuring point of pile B5.

Measuring point P2 was on edge pile B5, measuring point P5 was on secondary edge pile B6, measuring point P7 was on middle pile B7, and the height of three measuring points was 45 cm from the top surface of the adapter plate. Figure 19 shows the maximum hydrodynamic pressures at the three measuring points under the excitation of artificial waves 1 and 2. The hydrodynamic pressure on the edge pile B5 was the largest, followed by secondary edge pile B6, and the hydrodynamic pressure acting on the middle pile B7 was the smallest. Under artificial wave 1 excitation, the hydrodynamic pressures on piles B6 and B7 were 88.7% and 83.0% of those of edge pile B5, respectively. The ratios under artificial wave 2 excitation were 86.7% and 80.4%, which

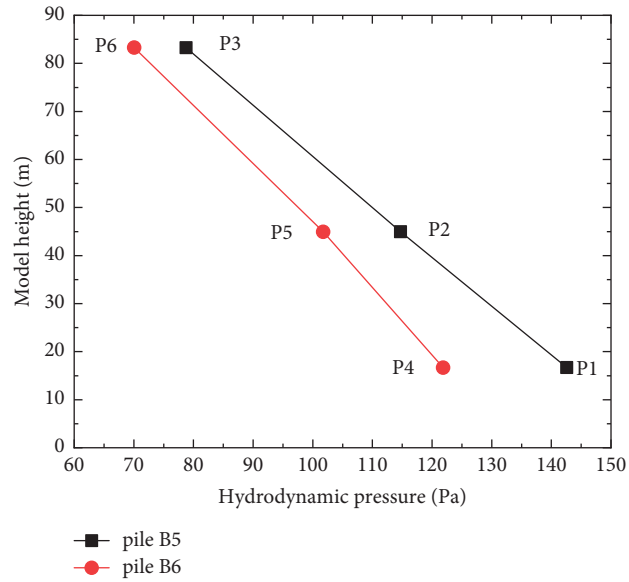

Figure 18: Comparison of hydrodynamic pressure experienced between piles B5 and B6.

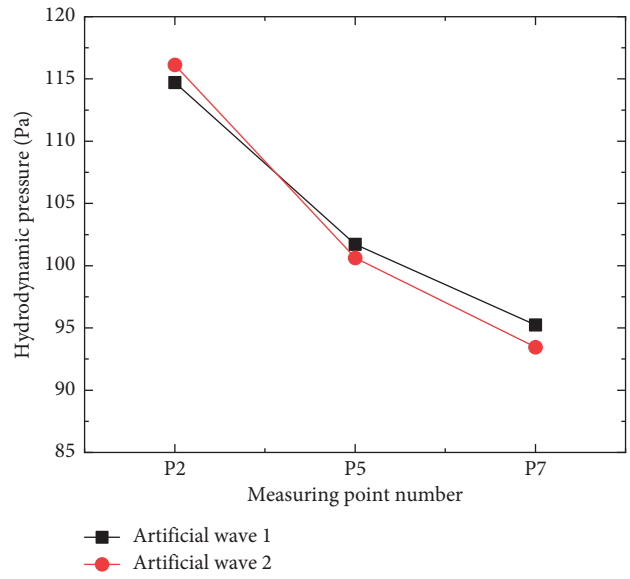

Figure 19: Comparison of hydrodynamic pressure experienced between outer pile and inner pile.

indicate that the hydrodynamic pressure acting on different piles under seismic excitation is different, and the magnitude of hydrodynamic pressure is related to the layout of the piles. The difference of hydrodynamic pressure for different piles is mainly due to the complex structure form and the interference between front- and back-row piles of the pile-cap foundation. Due to the resistance characteristics of pile-cap foundation in deep water, the front piles play a role in blocking the flow and will weaken the interaction between the water and back piles. Due to the cumulative shielding effect of front pile B5 and the second front pile B6, the hydrodynamic pressure of middle pile B7 is the minimum.

Under artificial wave 1 excitation along the X-direction, the hydrodynamic pressures on piles B6 and B7 were 88.7% and 83.0% of those of edge pile B5, respectively. The ratios under artificial wave 2 excitation were 86.7% and 80.4%, and cumulative shielding effect does not increase linearly, which indicates that the interaction between pile-cap foundation and the water is extremely complex.

Different from vibration of traditional single pile, the existence of adjacent piles changes the distribution of hydrodynamic pressure on each pile of pile-cap foundation, making the structure-water dynamic interaction more complicated. For the complex pile-cap foundation model of Xihoumen rail-cum-road bridge, the center distance between front pile and back pile is 0.21 m, the diameter of piles is 0.105 m, and the ratio is 2.0. According to the above-mentioned findings, the hydrodynamic pressure on the edge pile was the largest, followed by secondary edge pile, the hydrodynamic pressure on the middle pile was the smallest, and the maximum hydrodynamic pressure difference acting on the piles can reach approximately 20%. The experimental investigation results indicate that the influence difference of hydrodynamic pressure acting at different group piles needs to be considered in seismic analysis of complex deep-water pile-cap foundation.

3.3.3. Hydrodynamic-Pressure Analysis of Round-Ended Cap. To obtain the distribution law of the hydrodynamic pressure acting on the round-ended cap under X- and Y-direction excitations, a system study was conducted to analyze the maximum hydrodynamic pressure at seven measuring points arranged on the cap surface.

Under X-direction excitation of artificial waves 1 and 2, Figure 20 presents the maximum hydrodynamic-pressure distribution on the cap in 1.0 m water depth. For the seven measuring points, hydrodynamic pressure at measuring point P14 was evidently the maximum and its value was 96.7 Pa and 94.2 Pa, respectively, under X-direction excitation of artificial waves 1 and 2, and hydrodynamic pressure at measuring point P20 was close to measuring point P14 and the corresponding value was 94.1 Pa and 92.4 Pa, respectively. Hydrodynamic pressure at measuring point P17 was always the minimum. This is because measuring points P14 and P20 are at the front and measuring point P17 is at the side under X-direction excitation, and the hydrodynamic pressure presents a gradual declining trend from front to side. The maximum hydrodynamic pressure at measuring points P14 and P20 was 2.7 times the value of measuring point P17 under artificial wave 1 excitation. Under artificial wave 2 excitation, the ratios were 2.5 times and 2.6 times, respectively. The hydrodynamic-pressure ratio at the front and side measuring points reflects the influence of the cap section form on the velocity of the surrounding fluid particles.

Under the X-direction excitation of artificial waves 1 and 2, the hydrodynamic pressure at measuring point P15 was 87.2% and 84.8% of that at measuring point P14, and the hydrodynamic pressure at measuring point P16 was 47.4% and 46.5% of that at measuring point P14, which indicates

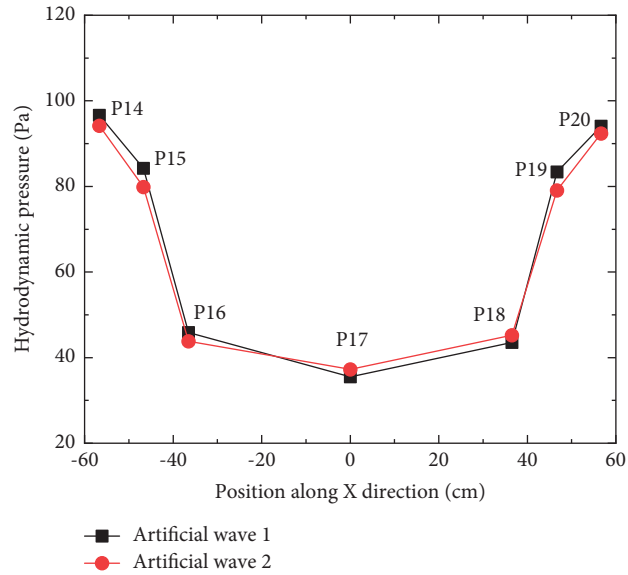

Figure 20: Variation in hydrodynamic pressure acting along the cap under X-direction excitation.

that hydrodynamic pressure decreased relatively slowly between measuring points P14 and P15, while it decreased rapidly between measuring points P15 and P16. Hydrodynamic pressure at measuring points P16, P17, and P18 was between 35.5 Pa and 45.8 Pa under X-direction excitation of artificial wave 1, whereas hydrodynamic pressure at measuring points P16, P17, and P18 was between 37.3 Pa and 45.3 Pa under X-direction of artificial wave 2. This indicates that the hydrodynamic pressure at measuring points P16–P18 was similar, and the amplitude change in the three measuring points at the side of the cap was relatively small.

Under Y-direction excitation of artificial wave 1 and 2, Figure 21 presents maximum hydrodynamic-pressure distribution on the cap in 1.0 m water depth. Measuring points P15–P19 are at the front and measuring points P14 and P20 are at the side. To compare with the hydrodynamic pressure under X-direction excitation, the same coordinate axis was used in Figures 20 and 21. The hydrodynamic pressure at measuring points P14 to P20 first increased and subsequently decreased gradually, and the variation trend of the hydrodynamic pressure acting along the round-ended cap was consistent under the Y-direction excitation of the two artificial waves. For the seven measuring points, the hydrodynamic pressure at measuring point P17 was the largest and its value was 107.7 Pa and 105.1 Pa under Y-direction excitation of artificial waves 1 and 2, respectively. The hydrodynamic pressure at measuring point P14 was the smallest, and that at measuring point P20 was similar to measuring point P14. The hydrodynamic pressure at measuring point P18 was 92.8% and 92.6% of that at measuring point P17, whereas the hydrodynamic pressure at measuring point P19 was 68.0% and 66.7% of that at measuring point P17. The hydrodynamic pressure at measuring point P20 was 53.9% and 51.9% of that at measuring point P17. The hydrodynamic-pressure distribution on the round-ended cap shows that hydrodynamic pressure decreased slowly

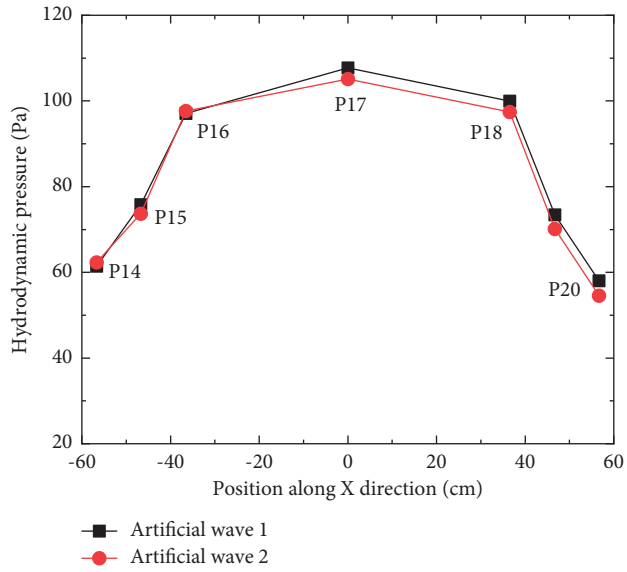

Figure 21: Variation in hydrodynamic pressure acting along the cap under *Y*-direction excitation.

between measuring points P17 and P18 but decreased rapidly between measuring points P18-P19 and P19-P20.

For seismic wave excitation in *X*- and *Y*-directions, the hydrodynamic pressure at the center of the seismic input direction was the largest, and the hydrodynamic pressure away from the seismic wave input direction gradually decreased. Although there are some differences between the hydrodynamic-pressure values on the cap under the excitation of the two artificial waves, the overall variation law was similar, and this is because the amplitudes of two artificial waves at the values of natural frequency of the test model are close. Under *Y*-direction excitation of artificial wave 1, the maximum hydrodynamic pressure at measuring point P17 was 1.8 times and 1.9 times that of measuring points P14 and P20, respectively. The ratio was 2.0 and 1.9 times, respectively, under the *Y*-direction excitation of the artificial wave 2. Compared with the *Y*-direction excitation, the maximum hydrodynamic pressure was significantly smaller, and the hydrodynamic-pressure ratio at the front and side was larger under *X*-direction excitation. The hydrodynamic pressure on the round-ended cap decreased faster from front to side. Viewed from the *X*-direction, the upstream surface of round-ended cap is composed of curved surface, which is relatively smooth. The fluid resistance effect of the cap under *X*-direction excitation was weaker, and the diversion role of curved surface was more conducive to the flow of fluid, which is advantageous for reducing the hydrodynamic pressure on the cap. Viewed from the *Y*-direction, the upstream surface of round-ended cap is composed of plane and curved surface, the contact area between the upstream surface and water is significantly larger and the normal direction of the plane coincides with the input direction of the artificial wave, and these factors will lead to greater hydrodynamic pressure on the upstream surface of the cap under the *Y*-direction excitation. It was observed that the hydrodynamic pressure on the cap was significantly affected by its shape. To reduce the hydrodynamic pressure on the cap and minimize the impact of the hydrodynamic pressure effect on the internal force of the pile-cap foundation, the shape of the large cap should be fully optimized in the seismic design of a deep-water pile-cap foundation.

3.4. Strain Analysis of Complex Pile-Cap Foundation Model. To study the mechanical characteristics of different piles of complex pile-cap foundations under earthquake excitation, the maximum tensile strain of piles under *X*- and *Y*-direction excitation was analyzed and discussed.

3.4.1. Strain Analysis of Different Piles under X-Direction Excitation. Artificial wave 1 was excited along the *X*-direction when the water depth was 0.0 m and 1.0 m, and the maximum tensile strain of side-row piles B1–B4 is shown in Figure 22. Whether subjected to 0.0 m or 1.0 m water depth, the maximum tensile strain of edge piles B1 and B4 is significantly larger than that of middle piles B2 and B3. The maximum tensile strain of edge pile B1 is 120.1 $\mu\varepsilon$ under 0.0 m water depth, the maximum tensile strain of middle pile B3 is 104.1 $\mu\varepsilon$, and the strain value of the latter is 86.7% of the former. The maximum tensile strain of edge pile B1 is 136.4 $\mu\varepsilon$ under 1.0 m water depth conditions, whereas the maximum tensile strain of middle pile B3 is 113.7 $\mu\varepsilon$ and the strain value of the latter is 83.4% of the former.

Artificial wave 1 was excited along the *X*-direction when the water depth was 0.0 m and 1.0 m, and the maximum tensile strain of middle-row piles B5–B9 is shown in Figure 23. Whether subjected to 0.0 m or 1.0 m water depth, the maximum tensile strain of edge pile B5 was always the largest, and that of middle pile B7 was always the smallest. The maximum tensile strain of middle pile B7 is 74.9% and 73.5% of that of edge pile B5 subjected to 0.0 m and 1.0 m water depths. The strain results of piles B1–B9 under *X*-direction excitation show that the maximum strain of different piles is clearly different. The strain value is related to the layout of piles, and the maximum strain difference of piles reached 26.4% at 1.0 m water depth. The main reasons for the above phenomena are as follows: complex pile-cap foundation is top-heavy because of the existence of large-sized cap, and the strain of each pile is the comprehensive result of eccentric vertical force and bending moment caused by the upper structure under earthquakes. The significant difference of the distance between each pile and the structure center and different eccentric effects of compression bending or stretch bending result in significant strain differences for each pile. Besides, the test results in Section 3.3.2 show that the hydrodynamic pressure acting on different piles varies under seismic excitation, the hydrodynamic pressure on the edge pile is the largest, followed by secondary edge pile, and the hydrodynamic pressure acting on the middle pile is the smallest, which is another important reason resulting in the strain difference of the piles in water.

Whether subjected to 0.0 m or 1.0 m water depth, the maximum tensile strain of side-row piles occurred in edge pile B1 and the corresponding value was 120.1 $\mu\varepsilon$ and

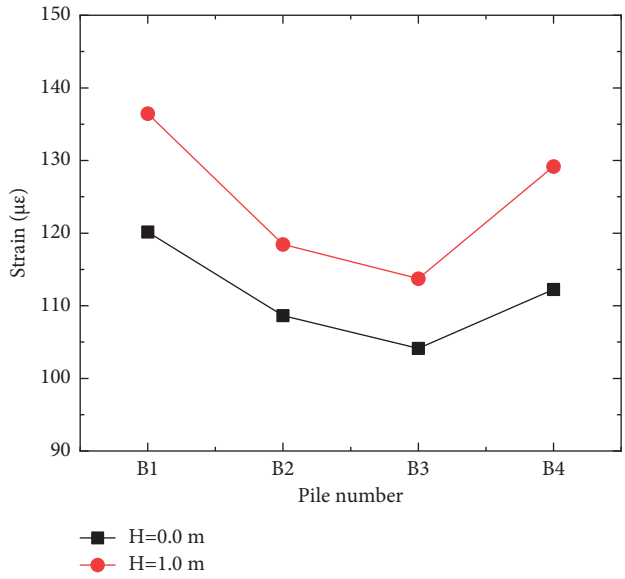

Figure 22: Maximum tensile strain of side-row piles.

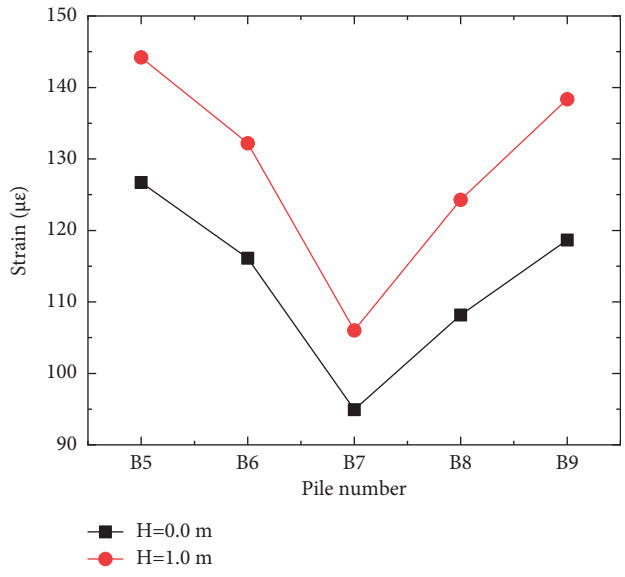

Figure 23: Maximum tensile strain of middle-row piles.

136.4 $\mu\varepsilon$, respectively. The maximum tensile strain of middle-row piles occurred in edge pile B5 and the corresponding value was 126.7 $\mu\varepsilon$ and 144.2 $\mu\varepsilon$, respectively. The pile-cap foundation is completely symmetrical about the X- and Y-axis. The edge piles B5 and B1 are located on the same side of the model, which conforms to the mechanical characteristics of the symmetric structure. The maximum tensile strain of edge pile B5 was 105.5% and 105.7% of edge pile B1 under 0.0 m and 1.0 m water depth; in both cases, the maximum tensile strain of edge pile B5 was greater. Viewed from the X-direction, edge piles B5 and B1 were more outward than other piles in the layout of eighteen piles. In particular, pile B5 was not only the front-row pile but also the edge pile, that is, pile B5 is a corner pile, which indicates that the corner pile of the pile-cap foundation distributes the largest load under seismic excitation, followed by the front-row pile, and the middle pile is the smallest.

In order to determine the scale for structural force and hydrodynamic force, a numerical analysis of prototype structure was conducted by using fluid-structure coupling model. When artificial wave 1 was excited along the X-direction, the horizontal force of the prototype structure without water was 152.4 MN, and the corresponding bending moment at the bottom of the pile-cap foundation was 7632.4 MN·m. The horizontal force of the prototype structure was 183.3 MN in 60 m deep-water environment, and the corresponding bending moment at the bottom of the pile-cap foundation was 8697.2 MN·m. Structural force was the main factor in the waterless condition; meanwhile, structural force and hydrodynamic force were the main factors in 60 m deep-water environment, and the influence differences in the waterless condition and 60 m deep-water environment were mainly caused by hydrodynamic force. Compared with the waterless condition, the horizontal force increased by 30.9 MN and the bending moment at the bottom of the pile-cap foundation increased by 1064.8 MN·m in 60 m deep-water environment, and the increase rates were 20.3% and 14.0%, respectively. According to the structure similarity criteria and fluid similarity criteria followed by the test design, the ratio of structural force and hydrodynamic force in the test model was consistent with the prototype structure.

It can also be seen from Figures 22 and 23 that the strain increment of nine piles caused by 1.0 m water depth was significantly different, and Table 4 presents the strain increment values and corresponding increase rate of the measuring points at the bottom of piles B1 to B9. The strain increase rates of nine piles are basically within 17% and the strain test results can also indirectly reflect structural force and hydrodynamic force, and the overall trend of the test results was consistent with abovementioned numerical calculation result. Piles B1, B4, B5, and B9 were the edge piles, and the corresponding strain increment was larger than that of the secondary edge pile and middle pile. According to the abovementioned findings of hydrodynamic pressure acting on different piles in Section 3.3.2, the hydrodynamic pressure acting on the edge pile was the largest, followed by the secondary edge pile, and the hydrodynamic pressure on the middle pile was the smallest. The hydrodynamic pressure difference was an important reason for the phenomenon that the strain increment of the edge piles was greater than that of the middle piles.

3.4.2. Strain Analysis of Different Piles under Y-Direction Excitation. Artificial waves 1 and 2 were excited along the Y-direction when the water depth was 1.0 m, and the maximum tensile strain at measuring points is shown in Table 5. For side-row piles under excitation of artificial waves 1 and 2, the maximum tensile strain of edge pile B1 was slightly greater than that of middle pile B2, and the corresponding strain values of middle pile B2 were 95.7% and 96.6%, respectively, of edge pile B1. For the middle-row piles under excitation of artificial waves 1 and 2, the maximum tensile

Table 4: The strain increment and increasing rate of nine piles caused by 1.0 m water depth.

Corresponding piles	B1	B2	B3	B4	B5	B6	B7	B8	B9
Strain increment ($\mu\varepsilon$)	16.3	9.8	9.6	17.0	17.5	16.1	11.1	16.2	19.7
Increasing rate (%)	13.6	9.0	9.2	15.1	13.8	13.9	11.7	15.0	16.6

Table 5: Maximum strain of piles under Y-direction excitation ($\mu\varepsilon$).

Loading wave	B1-S21	B2-S22	B5-S23	B6-S24	B7-S25
Artificial wave 1	148.2	141.9	119.6	114.6	107.5
Artificial wave 2	145.7	140.7	116.3	110.1	106.3

strain of edge pile B5 was the largest, secondary edge pile B6 was the second largest, and middle pile B7 was the smallest. The strain value of secondary edge pile B6 was 95.8% and 94.7% for edge pile B5, respectively, and the strain value of middle pile B7 was 89.9% and 91.4% of edge pile B5, respectively.

Under the excitation of artificial waves 1 and 2, the maximum tensile strain of edge pile B5 was 80.7% and 79.8% for edge pile B1, respectively. The strain results of side-row piles B1-B2 and middle-row piles B5–B7 under Y-direction excitation indicate that the maximum strain of different piles was clearly different. The maximum strain was related to the layout of piles; the maximum strain of the middle pile B7 of the middle row was 72.5% and 73.0% of the edge pile B1 of the side row under the excitation of artificial waves 1 and 2, respectively. The maximum strain difference of the piles reached 27.5% at 1.0 m water depth.

Viewed from the Y-direction, pile B1 was not only a front-row pile but also an edge pile, that is, pile B1 is a corner pile in the layout of eighteen piles, which indicates that the corner pile of the pile-cap foundation distributed the largest load under seismic excitation, followed by the front-row pile, and the middle pile was the smallest. This law is consistent with the strain characteristics of piles under the X-direction excitation. Therefore, strengthening the reinforcement of corner piles and front-row piles is recommended in the seismic design of a pile-cap foundation.

4. Conclusion

To study the mechanical characteristics of complex pile-cap foundations under earthquakes and the distribution law of hydrodynamic pressure acting on piles and caps in deep-water environments, a series of underwater shaking-table tests on complex pile-cap foundation were conducted. The main findings are summarized as follows.

(1) Considering the structure-water interaction, the existence of water can prolong the natural vibration period of complex pile-cap foundation, and the natural vibration period of complex pile-cap foundation increases by 2.1% for 0.5 m water depth and 5.6% for 1.0 m water depth. Differing from the previous studies, the acceleration of pile-cap foundation decreases by 2.6% for 0.5 m water depth and 4.2% for 1.0 m water depth, and the impact of water bodies on the acceleration depends on the acceleration response spectrum of the input seismic wave.

(2) The strain, displacement, and hydrodynamic pressure increased in varying degrees with water depths. The maximum strain occurred at the bottom of the piles, and the maximum at this location increased much faster with increasing water depths than the upper positions of the piles. Compared to the waterless condition, the maximum strain of the piles increased by 13.8% for the X-direction earthquake excitation and 15.1% for the Y-direction earthquake excitation in 1.0 m water-depth environment, and the influence of hydrodynamic pressure should be considered in the seismic design of complex deep-water pile-cap foundation.

(3) The strain of each pile under earthquake excitation is related to the layout of the piles. The maximum strain of the corner pile was the largest, followed by that of the front-row pile, and that of the middle pile was the smallest. The maximum strain difference of the different piles under the X- and Y-direction excitations reached 26.4% and 27.5%, respectively. It was recommended to strengthen the reinforcement of corner piles and front-row piles in the seismic design of a complex deep-water pile-cap foundation.

(4) The hydrodynamic pressure is closely related to the water depth. As the distance from the water surface decreases, the attenuation effect significantly increases. The hydrodynamic pressure acting on the piles gradually decreased from bottom to top. The surrounding piles can influence the hydrodynamic pressure of a certain pile, the hydrodynamic pressure acting on the edge pile was the largest, followed by the secondary edge pile, and the hydrodynamic pressure on the middle pile was the smallest. The maximum difference of the hydrodynamic pressure between the piles was 20%.

(5) Owing to the influence of the round-ended cap, the hydrodynamic pressure acting on the pile-cap foundation model suddenly increased at the cap. The hydrodynamic pressure anting on the cap gradually decreased from front to side, and the amplitude attenuation of the cap was significantly affected by its shape.

Based on complex deep-water pile-cap foundation for Xihoumen rail-cum-road bridge, the detailed data of dynamic response can be obtained from the test results, which provide the direct reference for the seismic design of actual bridge engineering. Experimental investigations discussed in this study clarify the weak point of complex pile-cap foundation under the earthquake and the influencing extent of the water depths on dynamic response. Besides, the

research results are helpful for revealing the mechanical characteristics of complex group-piles and the distribution rules of hydrodynamic pressure on different piles and cap in deep water. Nevertheless, due to the complexity of structure-water coupling problem for four or more rows of group piles and round-ended cap under earthquake action, some in-depth mechanisms can be further studied in future research.

Data Availability

The data used to support the findings of this study are included within the article.

Conflicts of Interest

The authors declare that they have no conflicts of interest.

Acknowledgments

This research was supported by the National Natural Science Foundation of China (11390361) and Major Project of "Science and Technology Innovation 2025" in Ningbo (2019B10076). The authors are grateful for the support.

References

[1] A. H. Moghaddam, H. Mazaheri, and M. Rabani Bidgoli, "Mathematical modelling, numerical analysis and damage of dams subjected to hydrodynamic pressure," *Ocean Engineering*, vol. 253, Article ID 111303, 2022.

[2] M. R. Shekari, S. M. Amiri, and M. R. Zareifard, "A numerical approach for coupled analysis of the seismic response of a cable-moored submerged floating tunnel," *Marine Structures*, vol. 83, Article ID 103156, 2022.

[3] F. Liang, X. Liang, and C. Wang, "Simplified added-mass model for evaluating the response of rectangular hollow bridge piers under earthquakes," *Journal of Bridge Engineering*, vol. 26, no. 10, Article ID 04021076, 2021.

[4] G. Yun and C. G. Liu, "A model for underwater shaking table tests on the basis of different similar criteria," *Applied Ocean Research*, vol. 118, Article ID 103010, 2022.

[5] J. Y. Chen, M. Wang, and S. Fan, "Experimental investigation of small-scaled model for powerhouse dam section on shaking table," *Structural Control and Health Monitoring*, vol. 20, no. 5, pp. 740–752, 2013.

[6] L. Martinelli, G. Barbella, and A. Feriani, "A numerical procedure for simulating the multi-support seismic response of submerged floating tunnels anchored by cables," *Engineering Structures*, vol. 33, no. 10, pp. 2850–2860, 2011.

[7] A. E. Dinçer, "Experimental and numerical investigation of hyper-elastic submerged structures strengthened with cable under seismic excitations," *European Journal of Environmental and Civil Engineering*, vol. 26, no. 9, pp. 4073–4092, Article ID 1837253, 2022.

[8] F. Li, X. Y. Peng, and W. Y. Huang, "Study on the effects of hydrodynamic pressure on the seismic responses of monopile embedded in deep water," *Earthquake Engineering and Engineering Dynamics*, vol. 42, pp. 70–79, 2022.

[9] B. Phansri, S. Charoenwongmit, E. Yooprasertchai, K. H. Park, P. Warnitchai, and D. H. Shin, "An experimental study on shaking table tests on models of a concrete gravity dam," *KSCE Journal of Civil Engineering*, vol. 19, no. 1, pp. 142–150, 2015.

[10] B. Phansri, S. Charoenwongmit, P. Warnitchai, D. Shin, and K. Park, "Numerical simulation of shaking table test on concrete gravity dam using plastic damage model," *Structural Engineering & Mechanics*, vol. 36, no. 4, pp. 481–497, 2010.

[11] H. Hazarika, E. Kohama, and T. Sugano, "Underwater shake table tests on waterfront structures protected with tire chips cushion," *Journal of Geotechnical and Geoenvironmental Engineering*, vol. 134, no. 12, pp. 1706–1719, 2008.

[12] A. Haddad, A. Barari, and R. Amini, "The remedial performance of suction caisson foundations for offshore wind turbines under seismically induced liquefaction in the seabed: shake table testing," *Marine Structures*, vol. 83, Article ID 103171, 2022.

[13] Q. H. Zhao, C. X. Li, and S. Dong, "Research status and prospect of seismic response of deep-water bridge pier," *Journal of Traffic and Transportation Engineering*, vol. 19, no. 2, pp. 1–13, 2019.

[14] G. Yun and C. G. Liu, "Shaking table tests on a deep-water high-pier whole bridge under joint earthquake, wave and current action," *Applied Ocean Research*, vol. 103, Article ID 102329, 2020.

[15] Z. X. Li, K. Wu, Y. Shi, L. Ning, and D. Yang, "Experimental study on the interaction between water and cylindrical structure under earthquake action," *Ocean Engineering*, vol. 188, Article ID 106330, 2019.

[16] X. Huang and Z. X. Li, "Influence of hydrodynamic pressure on seismic response of bridge piers in deep water," *China Civil Engineering Journal*, vol. 44, pp. 1–9, 2011.

[17] J. M. Song, K. Nam, Y. U. Sun et al., "Molecular and biochemical characterizations of a novel arthropod endo-beta-1,3-glucanase from the Antarctic springtail, Cryptopygus antarcticus, horizontally acquired from bacteria," *Comparative Biochemistry and Physiology Part B: Biochemistry and Molecular Biology*, vol. 155, no. 4, pp. 403–412, 2010.

[18] C. G. Liu and G. S. Sun, "Calculation and experiment for dynamic response of bridge in deep water under seismic excitation," *China Ocean Engineering*, vol. 28, no. 4, pp. 445–456, 2014.

[19] W. Lai, J. J. Wang, and X. Wei, "The Shaking table test for submerged bridge pier," *Earthquake Engineering and Engineering Vibration*, vol. 26, pp. 164–171, 2006.

[20] C. G. Liu, J. W. Zhang, and S. B. Zhang, "Model test on the underwater shaking table for the tower of deepwater cable-stayed bridge," *Journal of Water Resources and Architectural Engineering*, vol. 14, no. 3, pp. 118–123, 2006.

[21] J. T. Li, S. Q. Qin, and R. X. Zhang, "Developments and prospects of deep-water foundations for bridge," *Bridge Construction*, vol. 50, no. 3, pp. 17–24, 2020.

[22] Q. Li, L. Liu, and W. L. Yang, "Experimental and numerical investigation on pier-water coupling vibration of bridges in deepwater," *Engineering Mechanics*, vol. 33, no. 7, pp. 197–203, 2016.

[23] C. G. Liu, G. H Sun, and L. Han, "Validation of similitude laws for shaking table model test of dynamic interaction of water–pile-pier superstructure," *Journal of earthquake engineering and engineering vibration*, vol. 32, no. 4, pp. 13–18, 2012.

[24] Y. F. Liu, "Applicability analysis of rigid body assumptions of pile caps under earthquake," *Journal of Seismological Research*, vol. 37, no. 1, pp. 94–98, 2014.

[25] Y. K. He, B. Han, and W. Y. Ji, "Theoretical analysis of wave force on cap-pile group structure," *China Journal of Highway and Transport*, vol. 35, no. 11, pp. 31–38, 2022.

[26] X. Shu, Z. C. Chen, and L. G. Zhu, "Research on pile-cap system under torsional load," *Journal of Tongji University*, vol. 29, no. 5, pp. 515–519, 2001.
[27] China Communication Press, "Specifications for seismic design of highway bridges," China Communication Press, Beijing, China, JTG/T2231-01-2020, 2020.
[28] Y. Zhou, P. Xing, Z. Li et al., "Effect of occlusion site on the safety and efficacy of intravenous alteplase before endovascular thrombectomy: a prespecified subgroup analysis of DIRECT-MT," *Stroke*, vol. 53, no. 1, pp. 7–16, 2022.
[29] J. Zhang, K. Wei, and J. Z. Li, "Integrated assessment of the hydrodynamic added mass of the deep-water pile-cap foundation considering pile group-pile cap interaction," *Ocean Engineering*, vol. 244, Article ID 110418, 2022.
[30] C. Y. Liaw and A. K. Chopra, "Dynamics of towers surrounded by water," *Earthquake Engineering & Structural Dynamics*, vol. 3, no. 1, pp. 33–49, Article ID 4290030101, 1974.
[31] Q. Li and W. L. Yang, "An improved method of hydrodynamic pressure calculation for circular hollow piers in deep water under earthquake," *Ocean Engineering*, vol. 72, pp. 241–256, 2013.